Journal of Sound and Vibration 408 (2017) 210–219

Contents lists available at ScienceDirect

Journal of Sound and Vibration

journal homepage: www.elsevier.com/locate/jsvi

Design and experimental analysis of broadband energy harvesting from vortex-induced vibrations

L.B. Zhang [a], A. Abdelkefi [b], H.L. Dai [a,*], R. Naseer [b], L. Wang [a]

[a] Department of Mechanics, Huazhong University of Science and Technology, Wuhan 430074, China
[b] Department of Mechanical and Aerospace Engineering, New Mexico State University, Las Cruces, NM 88003, USA

ARTICLE INFO

Article history:
Received 6 March 2017
Received in revised form
13 July 2017
Accepted 15 July 2017
Handling Editor: L.G. Tham

Keywords:
Vortex-induced vibration
Energy harvesting
Synchronization
Softening behavior

ABSTRACT

In this paper, an operable strategy to enhance the output power of piezoelectric energy harvesting from vortex-induced vibration (VIV) using nonlinear magnetic forces is proposed for the first time. Two introduced small magnets with a repulsive force are, respectively, attached on a lower support and the bottom of a circular cylinder which is subjected to a uniform wind speed. Experiments show that the natural frequency of the VIV-based energy harvester is significantly changed by varying the relative position of the two magnets and hence the synchronization region is shifted. It is observed that the proposed energy harvester displays a softening behavior due to the impact of nonlinear magnetic forces, which greatly increases the performance of the VIV-based energy harvesting system, showing a wider synchronization region and a higher level of the harvested power by 138% and 29%, respectively, compared to the classical configuration. This proposed design can provide the groundwork to promote the output power of conventional VIV-based piezoelectric generators, further enabling to realize self-powered systems.

1. Introduction

In recent years, harnessing kinetic energy from ambient vibrations to generate electricity has attracted considerable attention due to its potential applications in operating portable, wearable, and implantable microelectronic devices [1–3]. For example, based on flow-induced vibrations or base excitations, significant effort has been devoted to create realization about a renewable and sustainable energy harvester using one of the transduction mechanisms, such as piezoelectric [4–8], electromagnetic [9,10], and electrostatic [11]. Among all, the piezoelectricity is one of the most attractive transfer mechanisms in mechanical energy conversion [12–14].

There are several aeroelastic phenomena that give rise to dynamic responses of the piezoelectric material structures subjected to wind loading, including galloping [15–18], vortex-induced vibration (VIV) [19–23], and flutter [24]. Among them, VIV-based energy harvesting has received increasing concerns due to its unique features of self-excited and self-restricted oscillations in the lock-in (synchronization) region as the vortex shedding frequency is close to one of the natural frequencies of the structure [25]. The concept of VIV-based energy converter was earlier proposed by Bernitsas et al. [26], who designed the device of vortex-induced vibration aquatic clean energy (VIVACE) which consists of a cylinder submerged

* Corresponding author.
E-mail address: daihulianglx@hust.edu.cn (H.L. Dai).

http://dx.doi.org/10.1016/j.jsv.2017.07.029
0022-460X/

perpendicularly to water flows. By virtue of wind flows, Akaydin et al. [27] investigated the performance of a piezoelectric energy harvester undergone VIV oscillations. Afterwards, Dai et al. [28] developed a distributed-parameter model and explored the effects of the parameters of structure dimensions and electrical load resistance on the output efficiency and performance of the VIV-based energy harvester. However, one of the main drawbacks in VIV energy harvesting is the narrow synchronization (lock-in) region and hence any fluctuation in wind speed results in a drastic decrease of the harvested power [29]. This to some extent restricts high efficient of energy harvesting from VIV.

Consequently, some researchers devoted to designing and proposing various techniques such as multimodal configurations [30], optimizing structural geometry [31] and adding small rods [32] to enhance the output performance and widen the synchronization region of energy harvesting systems. Yet there has been much interest in exploiting nonlinear restoring forces to increase vibration responses for high efficient energy harvesting [33–40]. One of the representative to utilize nonlinear restoring forces for energy harvesting was performed by Cottone et al. [41] who used two magnets and observed the bandwidth effect. Subsequently, the extensive and intensive investigations on nonlinear energy harvesters with monostable [42–44], bistable [45–51] and even tristable [52–54] characteristics have been studied to improve the efficiency of energy conversion over a wide operating excitation frequencies. Nevertheless, it should be mentioned that the above significant work almost focuses on energy harvesting from base excitations with introduction of nonlinear restoring or magnetic forces. Quite few studies employed such an approach for energy harvesting from flow-induced vibrations. Bibo et al. [55] designed a galloping energy harvester with nonlinear restoring forces and studied the effects of magnetic force coefficients on the cut-in speed and output performance. Recently, Huynh and Tjahjowidodo [56] simulated the VIV energy harvesting in bistable configurations by using spring components and found the chaotic responses of the harvester.

In this work, for the first time, we experimentally report an original effort to design high-efficient VIV-based piezoelectric energy harvesters using two magnets to provide a nonlinear restoring force, thus enabling to capture power across a broadband synchronization range of wind speed, which is not addressed before. For the sake of demonstrating broadband energy harvesting from VIV, a piezoelectric beam with a circular cylinder attached to its free end is fabricated and placed like a pendulum, with a small circular magnet (upper magnet) added on bottom of the cylinder. Another small circular magnet (lower magnet) is placed on the support which produces a repulsive force and can be adjusted in vertical and horizontal directions resulting in nonlinear magnetic forces, as shown in Fig. 1.

2. Experimental setup

The prototype of the energy harvesting system is shown in Fig. 1(b), which is subjected to cross flows (U) in the wind tunnel with a 35 cm $\times$ 35 cm test section. Under the action of vortex-induced force, the pendulum VIV-based energy harvester oscillates, alternatively bending the piezoelectric beam and hence generating a measureable voltage signal through an external electrical load resistance (R). The active length, width, and thickness of the piezoelectric beam are 62 mm, 10 mm, and 0.6 mm, respectively. The dimensions of the circular cylinder are 92 mm in length and 30 mm in diameter. The blockage ratio for the present experiments is about 11.7. A piezoelectric patch (MFC-M2807-P2, Smart Material Corp) is of negligible thickness and connected to the electrical load resistance in order to convert VIV oscillations to electrical power. The wind speed is measured by a Pitot tube anemometer and the generated voltage (V) across the load resistance is measured by the NI 9229 DAQ module.

It should be noted that the dynamics of the energy harvester can be affected with the introduction of magnets placed at a certain distance of Δx and Δy. Indeed, the magnets introduce a force dependent on Δx and Δy that opposes the elastic restoring force of the bended beam. Clearly, due to the magnetic force, the buckling instability of the piezoelectric beam can occur. This buckling effect is strongly dependent on the placement of the two magnets and hence the values of Δx and Δy.

3. Determination of damping and natural frequency for different cases

Firstly, the natural frequency and damping ratio of the proposed VIV-based energy harvesting system are obtained by free vibration tests for different cases, as shown in Tables 1 and 2, respectively. The damping ratio (ξ) for each case is obtained through the equation $\xi = \frac{\ln \eta}{\sqrt{4\pi^2 + (\ln \eta)^2}}$, in which η is the ratio between the vibration amplitudes of the former period and next period during free vibration tests. Indeed, due to the change of Δx and Δy, the natural frequency and damping ratio are lower or higher than those without magnet (case 1). It is noted that as $\Delta x = 0$, the natural frequency is decreased with the increase of Δy. This result can be explained due to the fact that all the considered Δy values are in the bistable (buckled) region. This case (when $\Delta x = 0$) is known by the presence of monostable and bistable regions depending on the placement between the two repulsive magnets. In the bistable region, it is known that a decrease of the spacing distance between the two repulsive magnets results in an increase in the natural frequency of the system which is the case in this study.

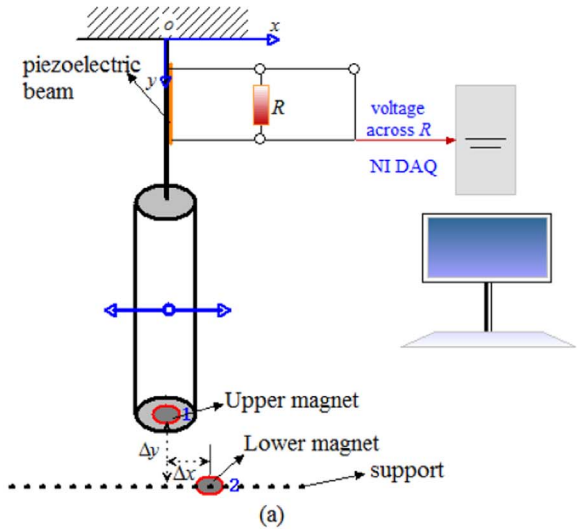

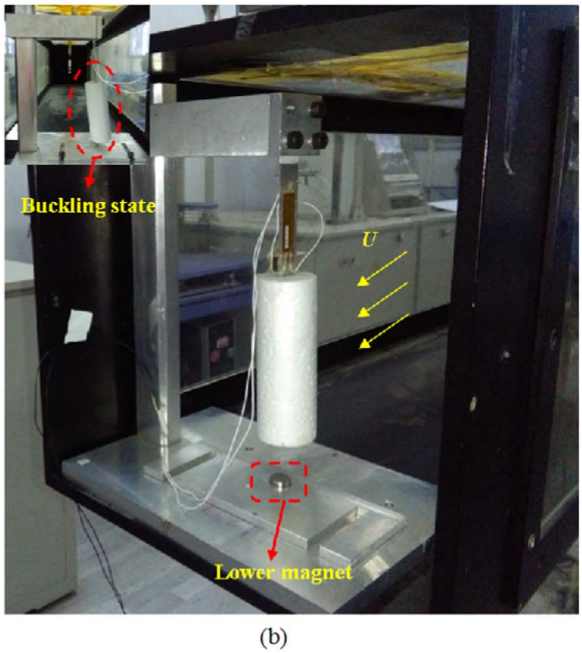

Fig. 1. (a): Schematic and (b): experimental setup of the proposed VIV-based energy harvesting system.

Table 1
Natural frequency of the proposed VIV-based energy harvester (by free vibration tests).

Natural frequency (Hz)	$\Delta x = 0$	$\Delta x = 10$ mm	$\Delta x = 20$ mm	Without magnet	One magnet
				(Case 1)	(Case 3)
$\Delta y = 5$ mm	30.0513	18.2174	10.9981	13.8528	10.9684
$\Delta y = 10$ mm	20.1626	16.0564	12.5087		
$\Delta y = 15$ mm	9.1533	13.9024	12.0078		

4. Performance of the designed harvester

In general, there exists a lock-in (synchronization) region where the energy harvester has a large vibration amplitude and hence generates high levels of average harvested power. Although increasing the load resistance results in an increase in the root mean square (RMS) voltage, there is an optimal load resistance at which the average harvested power is maximum. To

Table 2
Damping ratio of the proposed VIV-based energy harvester (by free vibration tests).

Damping ratio	$\Delta x = 0$	$\Delta x = 10$ mm	$\Delta x = 20$ mm	Without magnet	One magnet
				(Case 1)	(Case 3)
$\Delta y = 5$ mm	0.0044	0.0054	0.0111	0.0100	0.0115
$\Delta y = 10$ mm	0.0035	0.0056	0.0081		
$\Delta y = 15$ mm	0.0120	0.0062	0.0085		

determine this optimum value, three values of the wind speed (1.8 m/s, 2.0 m/s and 2.4 m/s for case 1; 2.2 m/s, 2.5 m/s and 3.0 m/s for case 2) are selected in the lock-in region for each of the two cases, namely, without magnet (case 1) and with magnets having $\Delta x = 10$ mm and $\Delta y = 5$ mm (case 2). The average power P_{avg} is obtained by the RMS voltage (V_{rms}) as: $P_{avg} = \frac{V_{rms}^2}{R}$, where $V_{rms} = \sqrt{\frac{1}{T_2 - T_1}\int_{T_1}^{T_2} V^2 dt}$. According to the expressions defined by Zhao et al. [57], in the present study, the values for the equivalent capacitance of the piezoelectric layer and the piezoelectric coupling coefficient are $C_p = 15.1$ nF and $\theta = 1.6 \times 10^{-5}$, respectively.

It follows from Fig. 2 that the optimal values of the load resistance for both cases with different wind speeds are concentrated between 300 kΩ and 700 kΩ. Outside this range of load resistances, the generated average power is clearly decreased. After intensive tests, it is found that it gives the highest output average power when the load resistance is around 500 kΩ. It should be stated that varying the values of Δx and Δy can change the natural frequency of the energy harvesting system, resulting in the variation of the optimal load resistance which can be a little lower or higher than the value of 500 kΩ. However, the present study focuses on the effects of nonlinear magnetic force on the performance of VIV-based energy harvesting. Therefore, we set the value of load resistance to be 500 kΩ in the rest of this study for convenient researches.

In order to further indicate the dynamic behavior of the cylinder, we plot in Fig. 3 the output RMS voltage as a function of wind speed in the case without magnets. Obviously, this characteristic behavior of the cylinder is typical and consistent with those reported for VIV responses from both theoretical and experimental aspects [21,27,28].

4.1. Effects of Δx and Δy on the energy harvester's performance

The performances of three VIV-based harvesters are evaluated by varying the wind speed between 1 m/s and 5 m/s, as shown in Fig. 4. The three considered energy harvesters are, namely, the classical case without attaching any magnet (case 1), the classical case with a magnet attached to the bottom of the cylinder (case 3), and the case with repulsive magnets having $\Delta x = 10$ mm and $\Delta y = 5$ mm (case 2). It is observed that with increasing the wind speed from 1 m/s to 5 m/s, there is a clear synchronization region for each case. As for case 1, the classical energy harvester without magnet, its lock-in region is between 1.7 m/s and 2.5 m/s and the peak average power is 116 μW. We note that as the wind speed is 2.1 m/s, there is a maximum output average power. The corresponding Reynolds number is about 4.8×10^3.

Concerning the energy harvester with magnets (case 2), its lock-in region is shifted to the right between 2 m/s and 3.5 m/s which is obviously widened compared to case 1. The harvested peak average power is also increased to 140 μW. These

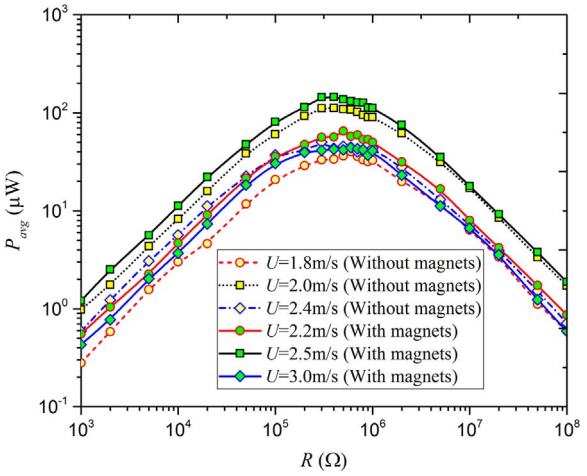

Fig. 2. Variations of the average harvested power as a function of the load resistance for two cases with different wind speeds. Case 1: without magnets; Case 2: with magnets when $\Delta x = 10$ mm and $\Delta y = 5$ mm.

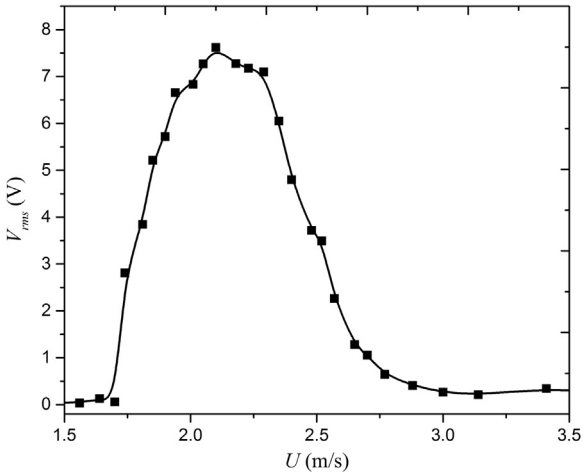

Fig. 3. Output RMS voltage as a function of wind speed in the case without magnets when $R = 500\,\text{k}\Omega$.

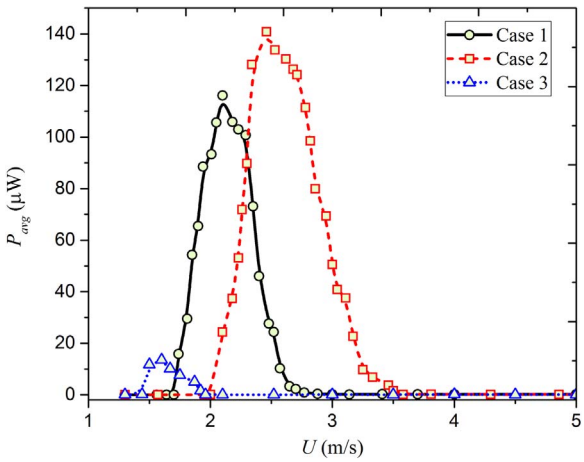

Fig. 4. Variations of average harvested power as a function of wind speed for three cases (case 1: without magnet; case 2: with magnets, $\Delta x = 10$ mm and $\Delta y = 5$ mm; and case 3: with upper magnet attached to the bottom of cylinder).

results are due to the increase in the natural frequency and decrease in the damping ratio of the energy harvesting system in case 2, as presented in Tables 1 and 2. It should be mentioned that the efficiencies of harvesting the peak power for case 1 (without magnets) and case 2 (with magnets) are approximately the same of about 0.6%. However, it is noted that the resonance region for case 2 is about between 2 m/s and 3.5 m/s which is larger than that for case 1 of about between 1.7 m/s and 2.5 m/s. This indicates the enhanced performance of efficiency from the aspect of broadband energy harvesting. As for the energy harvesting system when the magnet on the support is removed (case 3), it is found that the lock-in region is shifted to the left and the harvested power is sharply decreased compared to case 1. This result is predicted because the attached magnet on bottom of the cylinder results in a decrease in the natural frequency and an increase in damping ratio of the case 2 energy harvester. It follows from the plotted curves in Fig. 4 that the VIV-based energy harvesters in these three cases behave with almost a linear resonance characteristic. Indeed, no strong hardening or softening nonlinear behavior takes place. It should be mentioned that, in case 2, the VIV-based energy harvester displays a monostable feature due to the offset of lower magnet in the x direction. The results presented in Fig. 4 offer a general observation on the performance of VIV-based energy harvesting systems for different placements of the magnets.

To further investigate the effects of the introduced repulsive magnets to the energy harvester on its output performance, the distance between the two magnets is regulated to change the magnetic force acting on the VIV-based energy harvesting system. Clearly, the lock-in region and output performance are strongly dependent on the values of Δx and Δy. First, we set Δx to be equal to 20 mm, three values of Δy, namely, 5 mm, 10 mm and 15 mm are considered. It follows from Fig. 5(a) that $\Delta y = 10$ mm results in the highest average harvested power and widest lock-in region compared to its counterparts of $\Delta y = 5$ mm and 15 mm. This result is maybe due to the highest natural frequency and the lowest damping ratio for this case as shown in Tables 1 and 2. It should be stated that, compared to the performance of the classical VIV-based energy harvester (case 1), $\Delta x = 20$ mm produces a negative effect on the performance of the energy harvester from two sides, namely, the

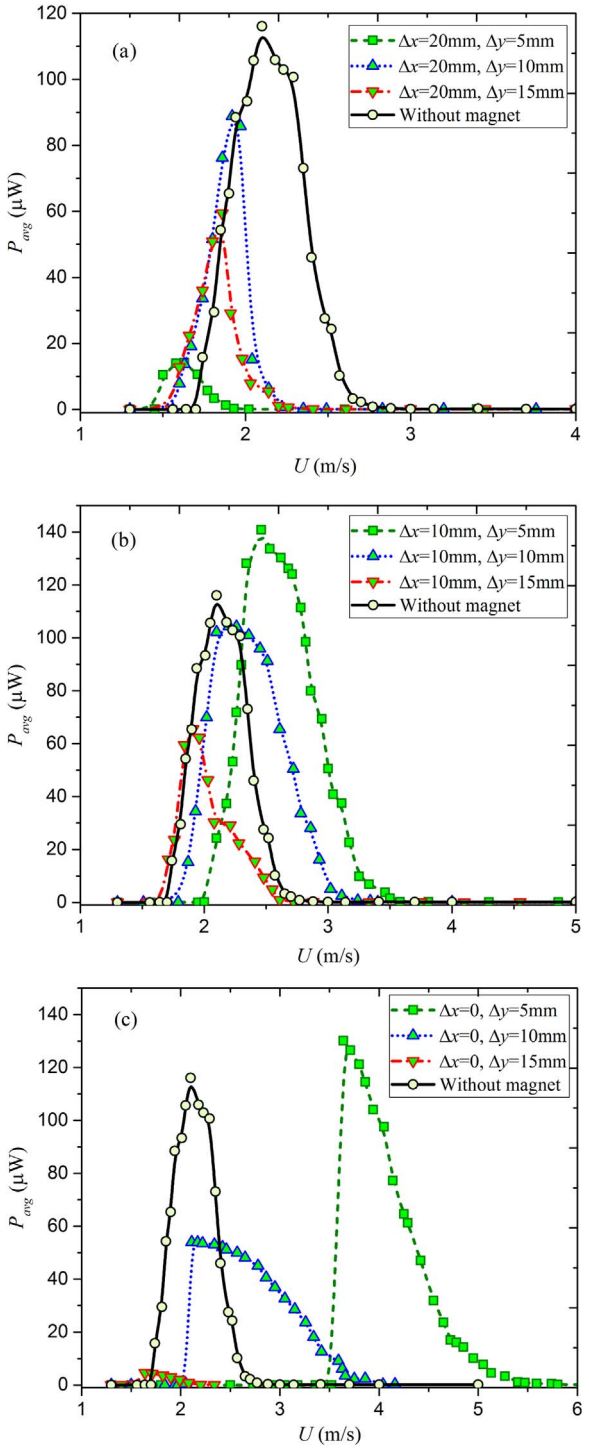

Fig. 5. Variations of average harvested power as functions of the wind speed for different values of Δx and Δy when the load resistance is 500 kΩ.

bandwidth of the lock-in region and the output level of harvested power. As a result, it is necessary to decrease Δx to enhance the nonlinear magnetic properties and hence the possibility of obtaining ultra-wide bandwidth VIV-based energy harvesters. When Δx is adjusted to 10 mm, it follows from Fig. 5(b) that the lock-in region shifts to the left and the corresponding output power is decreased with the increase of Δy from 5 mm to 15 mm. This can be expected due to the fact that there is a decrease in the natural frequency and an increase in the damping ratio of the energy harvester when Δy is increased. Apparently, the case of $\Delta y = 5$ mm brings the energy harvester a larger output power and wider lock-in region

than those without magnet which has addressed in Fig. 4. As Δy is increased to 10 mm, the energy harvester has a lower output average power than that without magnet but its lock-in region is widened. When Δy is increased to 15 mm, the performance of the energy harvesting system is not as good as that without magnet, which indicates $\Delta y = 15$ mm is not advisable.

It is interesting to investigate the performance of the VIV-based energy harvester in the scenario of $\Delta x = 0$, which is addressed in Fig. 5(c). It is observed that with increasing the wind speed, the output average power firstly jumps up to a peak value and then gradually decreases to low values. Clearly, it follows from the plotted curves in Fig. 5(c) that the energy harvester displays a softening feature of output power for the three considered values of Δy, and when Δy is smaller, this soften feature is clearer. This can be explained that the opposing magnetic force causes a periodic spring softening effect, thereby giving the harvester nonlinearities and increasing the response in a parametric amplification fashion.

Indeed, Δy is 5 mm and 10 mm, the lock-in region of the VIV-based energy harvester is shifted to the right and widened compared to that without magnet due to the increase in the natural frequency, as shown in Table 1. In addition, $\Delta y = 5$ mm gives a higher peak output power of 130 μW than that of 116 μW without magnet. Although $\Delta y = 10$ mm brings a lower output power, it results in a wider lock-in region. When Δy is increased to 15 mm, the performance of the energy harvester is negative from both aspects of lock-in region and output power levels. It can be concluded from Fig. 5 that when Δx is large, the VIV-based energy harvester displays monostable behavior based on the experimental observations. In this scenario, it exists an optimal distance of Δy that makes the output power maximum. However, in terms of bandwidth and performance of this designed energy harvester compared to the classical one (case 1), it is not beneficial. When Δx is a little smaller, in this scenario, the monostable feature has a better effect on the peak output power and bandwidth of lock-in region when Δy is small. As Δx is zero, the VIV-based energy harvester is in bistable state which results in a significant nonlinear softening characteristic, further leading to a wider lock-in region and higher output power that dependent on the value of Δy (spacing distance between the two repulsive magnets).

4.2. Further analysis for the energy harvester in the bistable region

It is noted that when $\Delta x = 0$, the VIV-based energy harvesting system owns bistable feature which easily induces nonlinear softening characteristic of dynamic responses. In this part, we focus on investigating the bistable state of the VIV-based energy harvester by increasing and decreasing the wind speed to capture the softening characteristic of dynamic responses. Firstly, the natural frequency and damping ratio of the energy harvester with different values of Δy between two repulsive magnets are analyzed, as shown in Fig. 6. It is observed that when the spacing distance between the two magnets is decreased (Δy is decreased), the natural frequency of the energy harvester is decreased first and then increased to higher values. The monostable region is defined by the values of Δy when the natural frequency is decreased to lower values when decreasing Δy. When Δy is decreased to lower values and the natural frequency starts to increase, this defines the bistable region. For this design, the critical values of Δy is around 18 mm. Theoretically, at the critical point of Δy when buckling takes place first, the natural frequency becomes zero. As for the damping ratio, it follows from Fig. 6 that it is increased first and then decreased. This indicates that the lowest natural frequency corresponds to the highest damping ratio of the energy harvesting system. It should be mentioned that the determination of the damping ratio is depending on the considered initial condition and an average value is considered based on the performed experiments.

Next, the increasing and decreasing bifurcation diagrams of the average harvested power for the three considered bistable configurations are plotted in Fig. 7. When $\Delta y = 5$ mm, during the process of increasing the wind speed, it is observed

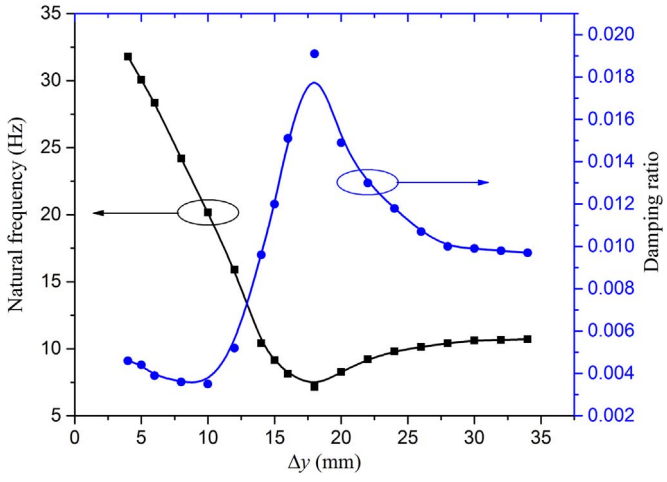

Fig. 6. Variations of the natural frequency (the black square) and damping ratio (the blue circle) as functions of Δy when $\Delta x = 0$. (For interpretation of the references to color in this figure legend, the reader is referred to the web version of this article).

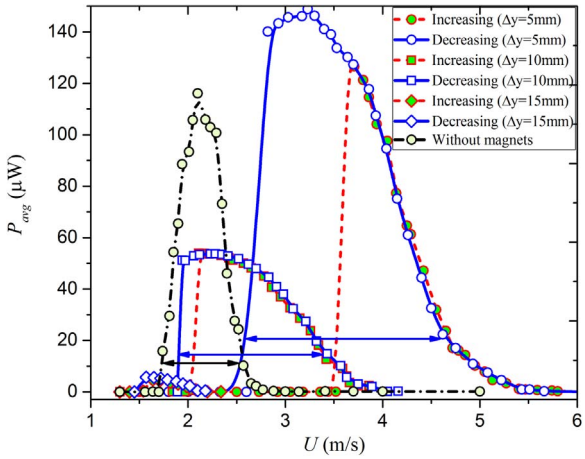

Fig. 7. Variations of harvested average power as functions of increasing and decreasing the wind speed for different values of Δy when $\Delta x = 0$.

that the harvested power is jumped from zero to the highest value when $U = 3.6$ m/s and then gradually decreased to zero with further increasing the wind speed to 5.5 m/s. When the wind speed is decreasing from 6 m/s, it is found that the harvested power is gradually increased to the highest value of 150 μW at 3.2 m/s and then slightly decreased to 140 μW at 2.7 m/s, finally it sharply drops to zero with further decreasing the wind speed. Indeed, the lock-in region of VIV energy harvesting for the case of $\Delta y = 5$ mm is between 2.7 m/s and 4.6 m/s, for the case of $\Delta y = 10$ mm is between 1.9 m/s and 3.4 m/s, while for the case without magnets is between 1.7 m/s and 2.5 m/s. Obviously, this nonlinear softening feature significantly increases the harvested power and the bandwidth of the lock-in region. When the spacing distance between

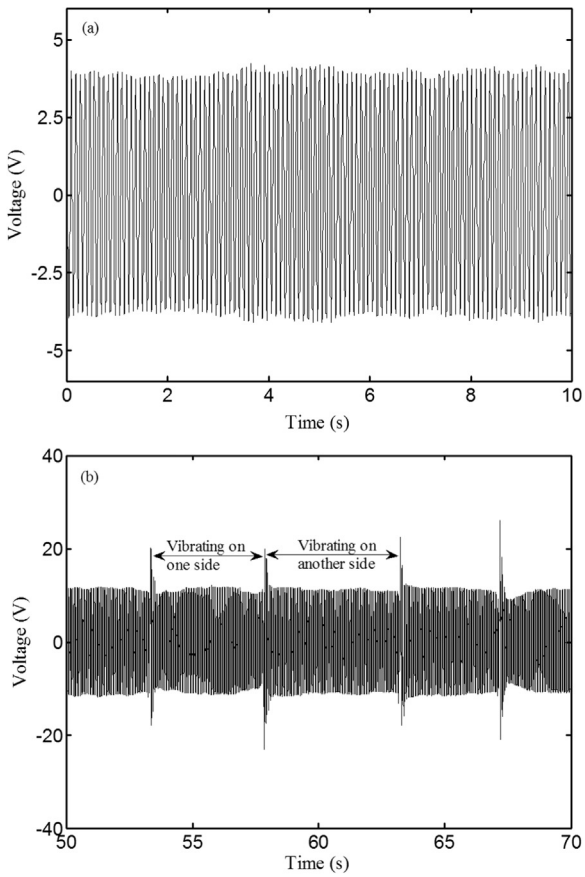

Fig. 8. Time histories of the output voltage for $\Delta x = 0$ in (a): the monostable case when $\Delta y = 25$ mm and $U = 1.7$ m/s and (b): the bistable case when $\Delta y = 5$ mm and $U = 3.4$ m/s.

the two repulsive magnets is increased, however, it is noted that the importance of the softening behavior becomes less pronounceable and hence narrow synchronization regions are observed. As Δy is further increased to beyond about 18 mm, the energy harvesting system becomes in a monostable configuration. In this way, we plot in Fig. 8 the typical time histories of output voltage for the harvester in monostable and bistable configurations. Inspecting Fig. 8(a) for the monostable configuration, we note the harvester system has just one equilibrium position around which the cylinder is oscillating. While for the bistable configuration, the harvester system has two equilibrium positions locating at both sides of $x = 0$. As a result, the cylinder can be alternately vibrating around the two equilibrium positions, as depicted in Fig. 8(b).

5. Conclusions

In summary, the present study has explored the improvement of energy harvesting by using the nonlinear magnetic forces which is beneficial for designing efficient and broadband VIV-based piezoelectric energy generators. It was demonstrated that the natural frequency of the energy harvester changes significantly with variation of the relative position of the repulsive magnets and hence the synchronization region is shifted. It was observed that the improved VIV-based energy harvester displays a softening behavior in the bistable region due to the introduced nonlinear restoring force, which greatly increases the output performance and lock-in region of VIV-based energy harvesting. The experimental results show that significant increments of 138% and 29% in the synchronization region and peak output average power are obtained compared to the classical configuration.

Acknowledgements

The authors gratefully acknowledge the support provided by the Fundamental Research Funds for the Central Universities, HUST (2017KFYXJJ135) and the National Natural Science Foundation of China (Nos. 11602090 and 11622216).

References

[1] D. Inman, B. Grisso, Towards autonomous sensing, in: Proceedings of Smart Structures and Materials Conference, SPIE, 2006.
[2] S. Roundy, P.K. Wright, A piezoelectric vibration-based generator for wireless electronics, Smart Mater. Struct. 13 (2005) 1131.
[3] A. Karami, D.J. Inman, Equivalent damping and frequency change for linear and nonlinear hybrid vibrational energy harvesting systems, J. Sound Vib. 330 (2011) 5583–5597.
[4] A. Barrero-Gil, G. Alonso, A. Sanz-Andres, Energy harvesting from transverse galloping, J. Sound Vib. 329 (2010) 2873–2883.
[5] Y. Yang, L. Zhao, L. Tang, Comparative study of tip cross-sections for efficient galloping energy harvesting, Appl. Phys. Lett. 102 (2013) 064105.
[6] A. Bibo, M.F. Daqaq, Energy harvesting under combined aerodynamic and base excitations, J. Sound Vib. 332 (2013) 5086–5102.
[7] H.L. Dai, A. Abdelkefi, L. Wang, Piezoelectric energy harvesting from concurrent vortex-induced vibrations and base excitations, Nonlinear Dyn. 77 (2014) 967–981.
[8] D. Vicente-Ludlam, A. Barrero-Gil, A. Velazquez, Enhanced mechanical energy extraction from transverse galloping using a dual mass system, J. Sound Vib. 339 (2015) 290–303.
[9] B.P. Mann, N.D. Sims, Energy harvesting from the nonlinear oscillations of magnetic levitation, J. Sound Vib. 319 (2009) 515–530.
[10] H.L. Dai, A. Abdelkefi, U. Javed, L. Wang, Modeling and performance of electromagnetic energy harvesting from galloping oscillations, Smart Mater. Struct. 24 (2015) 045012.
[11] D. Hoffmann, B. Folkmer, Y. Manoli, Fabrication, characterization and modelling of electrostatic micro-generators, J. Micromech. Microeng. 19 (2009) 094001.
[12] S.R. Anton, H.A. Sodano, A review of power harvesting using piezoelectric materials (2003–2006), Smart Mater. Struct. 16 (2007) 1–21.
[13] A. Erturk, D.J. Inman, Piezoelectric Energy Harvesting, Wiley, New York, 2011.
[14] A. Abdelkefi, Aeroelastic energy harvesting: a review, Int. J. Eng. Sci. 100 (2016) 112–135.
[15] A. Bibo, A. Abdelkefi, M.F. Daqaq, Modeling and characterization of a piezoelectric energy harvester under combined aerodynamic and base excitations, J. Vib. Acoust. 137 (2015) 031017.
[16] A. Abdelkefi, J.M. Scanlon, E. McDowell, M.R. Hajj, Performance enhancement of piezoelectric energy harvesting from wake galloping, Appl. Phys. Lett. 103 (2013) 033903.
[17] A.H. Alhadidi, M.F. Daqaq, A broadband bi-stable flow energy harvester based on the wake-galloping phenomenon, Appl. Phys. Lett. 109 (2016) 033904.
[18] G. Hu, K.T. Tse, K.C.S. Kwok, Enhanced performance of wind energy harvester by aerodynamic treatment of a square prism, Appl. Phys. Lett. 108 (2016) 123901.
[19] R. Song, X. Shan, F. Lv, T. Xie, A study of vortex-induced energy harvesting from water using PZT piezoelectric cantilever with cylindrical extension, Ceram. Int. 41 (2015) S768–S773.
[20] T. Cheng, Y. Wang, F. Qin, Z. Song, X. Lu, G. Bao, X. Zhao, Piezoelectric energy harvesting in coupling-chamber excited by the vortex-induced pressure, Appl. Phys. Lett. 109 (2016) 073902.
[21] H.L. Dai, A. Abdelkefi, Y. Yang, L. Wang, Orientation of bluff body for designing efficient energy harvesters from vortex-induced vibrations, Appl. Phys. Lett. 108 (2016) 053902.
[22] C. Grouthier, S. Michelin, E. de Langre, Optimal energy harvesting by vortex-induced vibrations in cables, in: Proceedings of the 10th International Conference on Flow-Induced Vibration (&Flow-Induced Noise), 2012.
[23] A. Barrero-Gil, S. Pindado, S. Avila, Extracting energy from vortex-induced vibrations: a parametric study, Appl. Math. Model. 36 (2012) 3153–3160.
[24] A. Erturk, W.G.R. Vieira, C. De Marqui, D.J. Inman, On the energy harvesting potential of piezoaeroelastic systems, Appl. Phys. Lett. 96 (2010) 184103.
[25] M.P. Paidoussis, S.J. Price, E. de Langre, Fluid-Structure Interactions: Cross-flow-induced Instabilities, Cambridge University Press, 2010.
[26] M.M. Bernitsas, K. Raghavan, Y. Ben Simon, E.M. Garcia, VIVACE (vortex induced vibration aquatic clean energy): a new concept in generation of clean and renewable energy from fluid flow, J. Offshore Mech. Arct. 130 (2008) 041101.
[27] H.D. Akaydin, N. Elvin, Y. Andreopoulos, The performance of a self-excited fluidic energy harvester, Smart Mater. Struct. 21 (2012) 025007.

[28] H.L. Dai, A. Abdelkefi, L. Wang, Theoretical modeling and nonlinear analysis of piezoelectric energy harvesting from vortex-induced vibrations, J. Intel. Mat. Syst. Struct. 25 (2014) 1861–1874.
[29] A.W. Mackowski, C.H.K. Williamson, On the energy harvesting potential of piezoaeroelastic systems, Phys. Fluids 25 (2013) 087101.
[30] A. Abdelkefi, A.H. Nayfeh, M.R. Hajj, F. Najar, Energy harvesting from a multifrequency response of a tuned bending–torsion system, Smart Mater. Struct. 21 (2012) 075029.
[31] F. Goldschmidtboeing, P. Woias, Characterization of different beam shapes for piezoelectric energy harvesting, J. Micromech. Microeng. 18 (2008) 104013.
[32] G. Hu, K.T. Tse, K.C.S. Kwok, J. Song, Y. Lyu, Aerodynamic modification to a circular cylinder to enhance the piezoelectric wind energy harvesting, Appl. Phys. Lett. 109 (2016) 193902.
[33] L. Gammaitoni, I. Neri, H. Vocca, Nonlinear oscillators for vibration energy harvesting, Appl. Phys. Lett. 94 (2009) 164102.
[34] A. Karami, D.J. Inman, Equivalent damping and frequency change for linear and nonlinear hybrid vibrational energy harvesting systems, J. Sound Vib. 330 (2011) 5583–5597.
[35] L. Tang, Y. Yang, A nonlinear piezoelectric energy harvester with magnetic oscillator, Appl. Phys. Lett. 101 (2013) 094102.
[36] M.F. Daqaq, On intentional introduction of stiffness nonlinearities for energy harvesting under white Gaussian excitations, Nonlinear Dyn. 69 (2012) 1063–1079.
[37] D.A.W. Barton, S.G. Burrow, L.R. Clare, Energy harvesting from vibrations with a nonlinear oscillator, J. Vib. Acoust. 132 (2010) 021009.
[38] R. Masana, M.F. Daqaq, Relative performance of a vibratory energy harvester in mono- and bi-stable potentials, J. Sound Vib. 33 (2011) 6036–6052.
[39] J.T. Lin, B. Lee, B. Alphenaar, The magnetic coupling of a piezoelectric cantilever for enhanced energy harvesting efficiency, Smart Mater. Struct. 19 (2010) 045012.
[40] A. Erturk, J. Hoffmann, D.J. Inman, A piezomagnetoelastic structure for broadband vibration energy harvesting, Appl. Phys. Lett. 94 (2009) 254102.
[41] F. Cottone, H. Vocca, L. Gammaitoni, Nonlinear energy harvesting, Phys. Rev. Lett. 102 (2009) 080601.
[42] S.C. Stanton, C.C. McGehee, B.P. Mann, Reversible hysteresis for broadband magnetopiezoelastic energy harvesting, Appl. Phys. Lett. 95 (2009) 174103.
[43] D. Barton, S. Burrow, L. Clare, Nonlinear oscillators for vibration energy harvesting, J. Vib. Acoust. 132 (2010) 021009.
[44] L. Gammaitoni, I. Neri, H. Vocca, Nonlinear oscillators for vibration energy harvesting, Appl. Phys. Lett. 94 (2009) 164102.
[45] A. Erturk, D.J. Inman, Broadband piezoelectric power generation on high-energy orbits of the bistable Duffing oscillator with electromechanical coupling, J. Sound Vib. 330 (2011) 2339–2353.
[46] S.C. Stanton, C.C. McGehee, B.P. Mann, Nonlinear dynamics for broadband energy harvesting: investigation of a bistable piezoelectric inertial generator, Phys. D 239 (2010) 640–653.
[47] M.F. Daqaq, Transduction of a bistable inductive generator driven by white and exponentially correlated Gaussian noise, J. Sound Vib. 33 (2011) 2554–2564.
[48] H. Vocca, I. Neri, F. Travasso, L. Gammaitoni, Kinetic energy harvesting with bistable oscillators, Appl. Energy. 97 (2012) 771–776.
[49] R.L. Harne, K.W. Wang, A review of the recent research on vibration energy harvesting via bistable systems, Smart Mater. Struct. 22 (2013) 023001.
[50] S.P. Pellegrini, N. Tolou, M. Schenk, J.L. Herder, Bistable vibration energy harvesters: a review, J. Intel. Mater. Syst. Struct. 24 (2013) 1303–1312.
[51] G. Litak, M. Borowiec, On simulation of a bistable system with fractional damping in the presence of stochastic coherence resonance, Nonlinear Dyn. 77 (2014) 681–686.
[52] J. Cao, S. Zhou, W. Wang, J. Lin, Influence of potential well depth on nonlinear tristable energy harvesting, Appl. Phys. Lett. 106 (2015) 173903.
[53] S. Zhou, J. Cao, D.J. Inman, J. Lin, S. Liu, Z. Wang, Broadband tristable energy harvester: modeling and experiment verification, Appl. Energy 133 (2014) 33–39.
[54] G.O. Tékam, C.K. Kwuimy, P. Woafo, Analysis of tristable energy harvesting system having fractional order viscoelastic material, Chaos 25 (2015) 013112.
[55] A. Bibo, A.H. Alhadidi, M.F. Daqaq, Exploiting a nonlinear restoring force to improve the performance of flow energy harvesters, J. Appl. Phys. 117 (2015) 045103.
[56] B.H. Huynh, T. Tjahjowidodo, Experimental chaotic quantification in bistable vortex induced vibration systems, Mech. Syst. Signal Process. 85 (2017) 1005–1019.
[57] L. Zhao, L. Tang, Y. Yang, Comparison of modeling methods and parametric study for a piezoelectric wind energy harvester, Smart Mater. Struct. 22 (2013) 125003.